

# Magnetic properties of photospheric regions with very low magnetic flux

H. Socas-Navarro

*High Altitude Observatory, NCAR<sup>1</sup>, Boulder, CO 80307-3000, USA*

navarro@hao.ucar.edu

and

J. Sánchez Almeida

*Instituto de Astrofísica de Canarias, E-38200, La Laguna, Tenerife, Spain*

jos@ll.iac.es

## ABSTRACT

The magnetic properties of the quiet Sun are investigated using a novel inversion code, FATIMA, based on the Principal Component Analysis of the observed Stokes profiles. The stability and relatively low noise sensitivity of this inversion procedure allows for the systematic inversion of large data sets with very weak polarization signal. Its application to quiet Sun observations of network and internetwork regions reveals that a significant fraction of the quiet Sun contains kilogauss fields (usually with very small filling factors) and confirms that the pixels with weak polarization account for most of the magnetic flux. Mixed polarities in the resolution element are also found to occur more likely as the polarization weakens.

*Subject headings:* line: profiles – methods: numerical – Sun: atmosphere – Sun: magnetic fields – Sun: photosphere

---

<sup>1</sup>The National Center for Atmospheric Research (NCAR) is sponsored by the National Science Foundation.

## 1. Introduction

The study of the quiet Sun magnetism is an open and challenging problem, particularly in the low magnetic flux limit ( $\sim 10^{17}$  Mx and below). From the observational point of view, two important difficulties must be overcome. First, the polarization signals are weak and therefore close to the noise level. This complicates the analysis of the observations with the currently available diagnostic tools. They employ non-linear least-squares fitting algorithms, which are usually very unstable in this regime. A second difficulty comes from the fact that the magnetic structures cannot be spatially resolved by present-day instrumentation. The measurement of magnetic properties has to be based on modeling. However, without a reliable physical model for the magnetic elements, the inference of atmospheric properties is uncertain. Any sensible diagnostic technique must necessarily rely on a proper understanding of the basic properties of the atmosphere (see, e.g., the discussion in Socas-Navarro 2001). The complication arises because both theoretical and observational arguments indicate that the magnetic field in the quiet solar photosphere may be intermittent with length scales much smaller than the mean free path of the photons (e.g., Sánchez Almeida et al. 1996; Sánchez Almeida 1998; Cattaneo 1999). In this situation the description of the basic properties of the atmosphere is not simple. The radiative transfer becomes non-trivial and absorption and emission must be properly averaged at each spatial point to synthesize spectra (Sánchez Almeida et al. 1996). The acronym MISMA (MIcro-Structured Magnetic Atmosphere) denotes an atmosphere with such small-scale magnetic inhomogeneities.

The problem of inverting Stokes profiles formed in MISMAs was addressed by Sánchez Almeida (1997), who developed an inversion code (IC) using a standard non-linear least-squares algorithm<sup>2</sup>. This code was applied by Sánchez Almeida & Lites (2000, hereafter SAL) to quiet Sun observations from the Advanced Stokes Polarimeter (Elmore et al. 1992). Since the polarization signal was too weak in most of the points of the observed map, SAL inverted only 15% of surface, where the polarization was above some arbitrary threshold. As a result, they obtained 5200 different model MISMAs that are capable of fitting the observations, even the most strikingly asymmetric ones, within a single framework.

Our work generalizes the study of SAL applying a novel inversion procedure to a larger fraction of the same observed region. By doing so, we extend the original results to weaker and therefore more numerous signals, thus improving the statistical significance of the con-

---

<sup>2</sup>The term *inversion code* stands for any procedure aimed at retrieving information on the physical conditions in the solar atmosphere by fitting observed quantities. The Stokes profiles describe the polarization of a spectral line, hence *inverting Stokes profiles* means inferring physical properties by reproducing the observed line polarization.

clusions. We also demonstrate the feasibility of the new technique to systematically retrieve information on the weak and very asymmetric line polarization produced by the quiet Sun, for which no other technique is available at the moment. The inversion technique is denoted by FATIMA (Fast Analysis Technique for the Inversion of Magnetic Atmospheres), and a brief is provided in §3.1. We begin this work by summarizing the observational material (§2). Then the specificities of the general inversion technique applied to our particular data set are described in §3.2 and §3.3. The main results are pointed out in §4, and their reliability is discussed in §5. Finally, we analyze in §6 the consequences to be drawn from the study.

## 2. Observations

The observations are summarized for the sake of comprehensiveness. Further details can be found in Lites et al. (1996) and SAL. The polarized spectra were gathered with the Advanced Stokes Polarimeter (Elmore et al. 1992; Lites et al. 1993) working on a very quiet  $57'' \times 90''$  region near disk center (Fig. 1). Scanning the map with a sampling interval  $\simeq 0''.38$  required some 9 minutes. Stokes  $I$ ,  $Q$ ,  $U$  and  $V$  profiles of the Fe I lines at  $6301.5 \text{ \AA}$  and  $6302.5 \text{ \AA}$  are available for every spatial position in the mapped region. Various tests indicate that the map reaches an angular resolution of about  $1''$ . The noise of the Stokes spectra is better than  $10^{-3} I_c$ ,  $I_c$  being the continuum intensity (see Figs. 2, 3 and 4). The Stokes spectra were corrected for instrumental polarization to a level below the noise (Skumanich et al. 1997). SAL inverted only those points of the region having a maximum Stokes  $V$  signal above an arbitrary threshold of  $3 \times 10^{-3} I_c$ . Some 5200 pixels or 15% of the mapped area satisfy this criterion. In this paper we extend the inversion to the entire map, although our analysis will be restricted to those points where the maximum Stokes  $V$  signal is at least twice the noise of each particular spectrum. Since the noise of the different spectra varies, this criterion optimizes the number of available spectra for a given signal to noise ratio. The noise is computed in a continuum window where no polarization is expected. We retain approximately 27% of the map for analysis.

## 3. Inverting the Stokes profiles

### 3.1. The inversion code

The Stokes data were inverted using FATIMA (see Socas-Navarro et al. 2001, hereafter SNLAL; Rees et al. 2000; López Ariste 2001). This IC is based on the Principal Component Analysis of the profiles, which extracts the most relevant features present in the spectra and

compares them to a database of synthetic profiles. The model atmosphere producing the synthetic profile in the database that is closer to the observed one is chosen as the solution of the inversion.

The main advantages and drawbacks of FATIMA with respect to other inversion procedures are discussed in detail by SNLAL. In particular, there are three important benefits that make it suitable for our purposes here:

1. Since it performs a global search over the whole space of possible models and profiles, FATIMA never settles on secondary minima. In this sense, it is very stable. If a discrepancy between the synthetic and observed profile is found, it must be ascribed to either the adopted physical scenario not being a valid description of the Sun or to the database not sampling the model hyperspace in an adequate manner.
2. As shown in SNLAL, FATIMA is relatively less sensitive to noise than other inversion codes. This is also related to the stability issues discussed above. Inversions based on iterative minimization algorithms are more likely to find secondary minima when faced to profiles with very low signal to noise ratio, like those analyzed in this work.
3. It is extremely fast, which results in the ability to process large data sets in a very short time.

An important point to bear in mind is that FATIMA does not solve the radiative transfer problem, and is therefore not bound to any particular type of model atmosphere. Instead, it simply relies on a precomputed set of models and profiles that are stored in a database. This means that it may be applied to any particular situation, independently of the physical ingredients that need to be taken into account, provided that the database has been constructed in a suitable manner.

### 3.2. The physical scenario

Although the emphasis in SNLAL was given on Milne-Eddington model atmospheres, FATIMA may also be applied to more sophisticated scenarios. One only needs to construct the database using profiles that are consistent with the model assumed. To this aim we used the models obtained by SAL from the MISMA inversion of the points with strongest polarization in the region described in §2.

The MISMA models consist of two magnetic components embedded in a non-magnetic background. The two magnetic components are allowed to have different magnetic field

strengths, polarity, mass flows, occupation fractions (fraction of occupied atmospheric volume), etc. These components are not monolithic structures. Instead, they represent the mean properties of a conglomerate of many different very narrow magnetic fluxtubes. The temperature stratification is forced to be the same inside and outside the fluxtubes. This is justified with the argument that the radiative energy exchange becomes an efficient smoothing mechanism that smears out any possible thermal imbalance in seconds (e.g., Spiegel 1957; Kneer & Trujillo-Bueno 1987; Stix 1991). Conservation of mass and magnetic flux is imposed in each magnetic component. Hence the magnetic field becomes weaker as the tubes spread with height, and the velocity amplitudes increase as the density drops. The tubes and the surrounding environment are in horizontal mechanical balance, i.e., at each height the magnetic pressure and gas pressure in the tubes is compensated by the gas pressure of the surroundings. Hydrostatic equilibrium is imposed in order to determine the density stratification of the tubes and the non-magnetic background. Since the velocities inferred from the observations are sub-critical, this should be a fairly good approximation. Finally, magnetic fields are assumed to be vertical, an assumption that does not limit the validity of the models. Should the structure be inclined, it produces the spectrum of a vertical structure except for a multiplying factor of the order of the cosine of the inclination (Sánchez Almeida & Trujillo Bueno 1999).

### 3.3. Application of FATIMA

The vertical magnetic fields in our model atmospheres do not produce linear polarization and therefore we do not consider Stokes  $Q$  and  $U$  in the fits.

Some of the techniques given by SNLAL to reduce the dimensionality of the problem are not applicable here because we are not dealing with Milne-Eddington model atmospheres. In particular, the scaling of the source function and the filling factor, which allows the IC to recognize similar profiles with different amplitudes, is not applicable here. For this reason, the database with the original synthetic profiles does not represent a valid statistical description of the whole observation, since it only contains the points with the strongest polarization signals. It exhibits an important bias, and FATIMA will be unable to provide good fits to many profiles. To overcome this difficulty, we have set a global magnetic filling factor as a parameter that affects all MISMA components in the same way. FATIMA selects the model atmosphere in the database producing the synthetic Stokes profiles  $\{I_i, V_i\}$  that minimizes the residuals

$$\chi^2 = \sum_i \left\{ \left[ \frac{V_{oi}}{V_o^m} - \frac{V_i}{V^m} \right]^2 + [I_{oi} - I_i]^2 \right\}. \quad (1)$$

The index  $i$  varies with wavelength, whereas the set  $\{I_{oi}, V_{oi}\}$  represents the observations. The Stokes  $V$  profiles, both synthetic and observed, are normalized in equation (1) to their extreme values  $V^m$  and  $V_o^m$ . The scaling factor is then given by

$$\alpha = V_o^m / V^m. \quad (2)$$

Once the best fitting profile is found in the database, the filling factor of the individual MISMA components in the original model is multiplied by the global filling factor (2) to render the best fitting model atmosphere.

By accepting such scaling, we assume that the filling factors involved are much smaller than unity, which is the case here. Moreover, it is also assumed that the original spectra inverted by SAL represent an adequate sample of all the line shapes that may be found in the entire map. They only exhibit stronger polarization because, statistically, the magnetic components are present with a larger filling factor in those points. This is a reasonable assumption since the classification into low or high signals carried out by SAL does not obey physical differences, but it results from an arbitrary thresholding relative to the noise of the observations. In addition, the extrapolation is rather modest affecting polarization signals that are at most a factor three weaker than the weakest in the database. If this scaling does a proper job, then the modified version of FATIMA should be able to provide good fits to the observations over the whole map, including the line asymmetries. As we discuss in §4.1, this is indeed the case. All observations are successfully inverted with this scenario, and we are able to obtain a model MISMA for each pixel.

The telluric lines in the observed spectral region were removed from the intensity spectra before proceeding with the inversion. This was accomplished by interpolating between two points far in the wings of these lines. Ideally, these distant points should be in the continuum. In our case, however, the Fe I lines of interest are too close in wavelength, which results in a slight deformation of the Fe line wings. This effect has negligible impact on the inversions, because both the synthetic and the observed profiles have been clipped in exactly the same manner, and also because most of the information retrieved is contained in the Stokes  $V$  profiles, which are not affected by the telluric lines.

## 4. Results

When FATIMA runs on the observed map, we obtain a model MISMA and a synthetic profile for each pixel. Then we select only those points fulfilling the criterion described in §2 which left approximately 27% of the surface available for study. For all these points we have the variation with height in the atmosphere of the relevant physical parameters (from

magnetic fields to temperatures). Some general trends of these properties are described in the forthcoming sections.

#### 4.1. Quality of the fits

The overall quality of the fits is very good, in the sense that all observed profiles are well reproduced within the noise level. Figures 2 to 4 show some representative examples of different fits to observations with various signal levels. In particular, the synthetic profiles reproduce all sorts of Stokes  $V$  asymmetries, a fact already known for the strongest polarization signals analyzed by SAL, but which remains valid for the weak signals studied here. Therefore, the assumption that our database is representative of the whole data except for the effect of a global filling factor, is justified *a posteriori* (see §3.3).

#### 4.2. Magnetic field strength

Figure 5 shows a map of the average unsigned magnetic field strength at the base of the quiet Sun photosphere (i.e., the height where the continuum optical depth at 5000 Å equals unity or the total pressure becomes  $1.3 \times 10^5 \text{ dyn cm}^{-2}$ ). We represent the mean field strength of the two magnetic components in the resolution element (a density-weighted mean that mimics the result to be obtained if a single field strength were assigned by the IC; see Sánchez Almeida 2000). The network may be easily recognized as patches of strong field whose centers match the signals observed in the magnetogram (Fig. 1). These patches are much larger than their counterpart in the magnetogram, indicating a large decrease of occupation fraction towards the cell interiors (see also Fig. 6). Even outside the network most of the pixels harbor magnetic fields stronger than 1 kG. However, they tend to be slightly weaker than those around network patches. Among the Inter-Network (IN) fields, we find a few intrinsically weak sub-kG fields. The weakest fields tend to appear in the external parts of magnetic structures having larger field strengths, although the converse is not true. Frequently magnetic structures become below the observational threshold with no transition through a weakening of the field strength.

Figure 7 shows the magnetic field strength versus the magnetic flux density of the observation. The latter is defined as the total magnetic flux across the pixel divided by the area of the pixel, and it is supposed to be the quantity shown in magnetograms (e.g. Keller et al. 1994). As one moves towards weak flux densities (i.e., weak polarization signals), the mean field slightly decreases and, simultaneously, the scatter of possible values increases.

Still, most pixels show kG fields. We argue in §5 that these field strengths are not an artifact of the inversions but real. However, measurements with the IR Fe I line at 15648 Å convincingly show sub-kG fields associated with the IN fields (see Fig. 7), which leads to the conclusion that both weak and strong fields have to co-exist within regions 1'' across. We consider this point in §6 below.

### 4.3. Magnetic flux

Figure 8 shows the total (unsigned) magnetic flux of the region when all those pixels above a given level of Stokes  $V$  signal are considered. In agreement with SAL, the amount of magnetic flux in the region keeps increasing as the sensitivity improves, with no clear signs of saturation. The total flux of the region in the pixels that we analyze amounts to  $4.8 \times 10^{20}$  Mx. The mean flux density, corresponding to the total flux over the total area of the region, is 18 G. If one employs only points outside the network (defined as those with a occupation fraction smaller than 10%), the flux density decreases to 10 G.

These values for the magnetic flux and magnetic flux density are large in various senses. SAL obtained for the same region  $3.3 \times 10^{20}$  Mx when only the strongest signals are considered. We gain a factor two in sensitivity which produces a 50 % increase of the magnetic flux. It is clear how the sensitivity of the observation plays a crucial role in the determination of the quiet Sun magnetic flux budget (and therefore the energy budget).

On the other hand, we also computed the flux density of the map from the magnetogram in Figure 1 following the standard procedure to calibrate magnetograms<sup>3</sup>. The total flux thus obtained is  $2.0 \times 10^{20}$  Mx, which infra-estimates the flux by a factor 2.4. This deficit can be pinned down to various factors: the saturation of the Fe I 6302.5 Å line whose circular polarization is no longer proportional to the magnetic flux for kG fields (e.g. Stenflo 1973), the weakening of the lines in magnetic concentrations (Harvey & Livingston 1969), but also to the partial cancellation of the existing flux. Two opposite polarities frequently coexist in the resolution elements. Figure 9 shows the fraction of pixels where two opposite polarities in the resolution elements are invoked to reproduce the observed polarization.

The amount of flux in the quiet Sun is also large as compared to the flux observed in active regions during the solar maximum. Should the full Sun be covered by quiet regions like the one we study, the total unsigned flux across the solar surface would be  $10^{24}$  Mx,

---

<sup>3</sup>We use equation (3) below with the derivative computed using the mean Stokes  $I$  profile observed in the entire region. This leads to a calibration constant of 5145 G per Stokes  $V$  signal unit.



which is similar but larger than the magnetic flux during the solar maximum measured with standard low spatial resolution magnetographs (see Schrijver & Harvey 1994, Fig. 3). This fact indicates that taking into account the contribution of the IN fields may be important to evaluate and characterize the flux budget during the cycle, including the evolution with time.

#### 4.4. Mass motions

The observed asymmetric Stokes  $V$  profiles (Figs. 2, 3 and 4) follow from a rather simple velocity field. The magnetic components are embedded in a downflowing non-magnetic environment. The two magnetic components exhibit different motions. One of them is almost at rest and contains most of the magnetized mass. The other one tends to undergo strong downflows.

The distribution of velocities at the height corresponding to the base of the non-magnetic photosphere is shown in Figure 10. It contains the mean and the standard deviation as a function of the flux density. We separate the two components according to the velocities. The mean of the distribution in the slow component (the solid line) is very small for large magnetic flux densities. In fact, it is smaller than the uncertainty given by the absolute wavelength calibration (refer to SAL). The scatter is also small in this region of the diagram. As we move to lower flux densities (say below 10 G), the distribution shifts to negative (upwards-directed) velocities and the scatter increases slightly. The second component (the dashed line) is characterized by important downflows of  $\simeq 3 \text{ km s}^{-1}$  at this height. Its mean value remains approximately constant over the whole range of flux density values, but in this case the scatter grows significantly when we consider weak signals.

#### 4.5. Occupation fraction

Figure 6 shows the occupation fraction, i.e., the fraction of volume in the resolution element occupied by magnetic fields. The map corresponds to the lower photosphere. Occupation fractions span from some 20%, for a few network concentrations, to 0.5%, for the weakest polarizations analyzed here. The mean value for the surface that we analyze is about 4%. If the network concentrations are not considered (a discrimination based on the polarization threshold used in §4.3), it decreases to 3%. If one considers the whole region instead of the 27% having reliable signals, then the magnetic fields that we detect occupy only 1% of the total volume. This figure is a lower limit because it assumes that places with

negligible signal contain no magnetic field.

## 5. Reliability of the results

This work employs an unusual method of inversion to analyze low polarization signals. Since the reliability of our conclusions is very much based on the dependability of the inversions, we feel compelled to explain in some detail the studies that give us confidence on the results.

First, we compared the model atmospheres chosen by FATIMA for those points used to produce the database. In 90% of these points, the field strength retrieved by FATIMA differs less than 10% from the value in the database, which proves that the IC is working properly in the five thousand cases where we can test it directly. In particular, it shows that the principal component decomposition of the profiles does not seem to introduce artifacts.

Second, we wondered whether the noise of the observation was too high so that the IC has no information and it assigns model atmospheres at random. Several arguments discard such concern. The probability of finding a given physical property in the whole region is not the same as that obtained from the points in the database. Should atmospheres in the database were chosen at random, the distributions of magnetic field strength, velocities, etc, would have to mimic the original one. However, this is not the case. Magnetic fields are sensibly weaker in the whole region, the fraction of opposite polarities larger, and so forth. Figure 9 shows the fraction of times that FATIMA assigns mixed polarities in the resolution element. It becomes 35% in the weakest signals analyzed here whereas, in average, only 13% of the times such mixed polarities are present in the original database.

Another hint that the IC is not assigning magnetic properties at random can be inferred from Figure 5. Note that neighboring pixels show similar field strengths although the inversions of all of them are independent. Since adjacent pixels show similar profiles, this indicates the IC has been able to distinguish their shapes and separate them.

Third, one of the important conclusions of the work is the ubiquity of kG field strengths even outside the network. Since most of the magnetic fields in the database correspond to kG (SAL, Fig. 14), one naturally wonders whether this bias determines the conclusion. It does not. The database also contains sub-kG fields, but most of the times they are left aside on purpose by the IC. There is enough information in the observed profiles to distinguish between kG and sub-kG fields. Most of the profiles observed in IN regions cannot be produced by sub-kG fields. An example of how the fits worsen if one attempts sub-kG field fittings in a region whose best fit requires kG is shown by Sánchez Almeida (2001), §4. Here we

offer a much simpler argument pointing in the same direction. Suppose that the IN fields were covered by intrinsically weak fields of the kind inferred in the IR (Lin & Rimmele 1999; Collados 2001). These fields are weak in two different senses. The radiative transfer can be treated in the so-called *weak field approximation*, i.e., the Stokes  $V$  scale with the wavelength derivative of the intensity profile,

$$V(\lambda) = -k g_{eff} \lambda_0^2 B \frac{dI(\lambda)}{d\lambda}, \quad (3)$$

where  $k$ ,  $g_{eff}$ ,  $\lambda_0$  and  $B$  have their usual meanings (a constant, the effective Landé factor, the mean wavelength of the spectral line, and the longitudinal component of the magnetic field, respectively). On the other hand, the magnetic fields are *dynamically weak* so that they cannot determine the thermodynamic properties of the atmosphere. This second argument points out that in weak magnetic structures, the thermodynamic properties have to be close to those of the quiet Sun, so that the relative strengths of Fe I 6302.5 Å and Fe I 6301.5 Å are those observed in the quiet Sun. Consequently, for intrinsically weak fields, the Stokes  $V$  signals have to be given by equation (3),  $I$  being the quiet Sun spectrum  $I_q$ . Figure 11 shows the product  $g_{eff} dI_q(\lambda)/d\lambda$ . It is clear how the signal to be expected in Fe I 6301.5 Å is much weaker than that in Fe I 6302.5 Å, as it is indeed observed in some places (see Fig. 4). However, observations usually show the two lines with similar degrees of polarization (Fig. 3), proving that the lines are formed outside the weak field regime, which corresponds to kG. Figure 12 displays the scatter plot of the maximum Stokes  $V$  signals observed in the two Fe I lines employed in the study. Note how most of them appear clearly above the line corresponding to weak fields, as deduced from the derivatives in Figure 11. In short, despite the uncertainties of the inversion, the presence of kG fields in the IN is a solid result.

## 6. Conclusions

We investigate the properties of quiet Sun regions having very small magnetic flux (down to the smaller that we can detect, equivalent to a few times  $10^{16}$  Mx; see Fig. 7 and Fig. 10). These regions, frequently referred to as “non-magnetic” regions, occupy most of the solar surface and therefore they may easily contain a sizeable fraction of the photospheric magnetic flux and energy (e.g., Stenflo & Lindegren 1977; Yi et al. 1993; Sánchez Almeida 1998). Both observations and theory suggest that the fields of the quiet Sun have a very complex topology (e.g. Cattaneo 1999; SAL), which hinders an easy detection. The tangling of field lines cancels to a large degree the polarization that would reveal the presence of

magnetic structures<sup>4</sup>. Many of the weakest signals appear in the network cell interiors; the so-called Intra-Network fields (IN). Although the first detections of weak IN fields date back to the seventies (Livingston & Harvey 1971; Livingston & Harvey 1975; Smithson 1975), we still have a very rudimentary knowledge of their basic properties. Low angular resolution magnetograms have provided information on their apparent shapes, magnetic fluxes and macroscopic motions (e.g., Wang et al. 1995; Zhang et al. 1998, and references therein.) However, the advent of a generation of spectro-polarimeters with improved sensitivity has provided new data that remain to be incorporated into a consistent paradigm.

One of the first and important results of the new polarimeters has been finding very asymmetric Stokes profiles (Sánchez Almeida et al. 1996; Grossmann-Doerth et al. 1996; Sigwarth et al. 1999; SAL). Obviously, the observed polarization is produced in atmospheres that require more than a single magnetic field and a single velocity to be described. The inference of the physical properties of such atmospheres requires special inversion techniques. This inference presents an additional complication, namely, the observed polarization signals are low and therefore close to the noise level. In this work we propose, essay and then use a new technique that copes with these two difficulties. It reproduces the asymmetries of all observed Stokes profiles (§4.1). The application of the technique allows us to obtain model atmospheres for 27% of the observed quiet Sun region. The procedure is a modification of FATIMA (SNLAL; see §3.1 and 3.3) which employs a database of synthetic observations based on the MISMA inversion of the strongest signals in the region (SAL). This inversion technique is extremely fast, and it offers a real chance to handle large data sets of very weak asymmetric polarization signals, like those presumably needed for the analysis of future observations.

The inversions show that most polarization signals in the quiet Sun correspond to kG fields at the base of the photosphere (§4.2 and Fig. 5). This is in agreement with previous observations based on Fe lines in the visible spectral range (Grossmann-Doerth et al. 1996 ; see, however, Keller et al. 1994), and we show this conclusion to be a solid result of our analysis (§5). On the other hand, different observations based on the Fe I IR line at 15648 Å almost exclusively find sub-kG fields in regions having similarly low flux densities (Lin 1995; Lin & Rimmele 1999; Collados 2001). Again this is a robust conclusion mostly based on the separation of the Stokes  $V$  peaks whose small splitting does not correspond to kG fields. We believe that the apparent contradiction between visible and IR based field strengths is not real. As explained by SAL (§4.5), the IR observations are not sensitive to the kG fields that may exist. The two seemingly inconsistent observations actually indicate that various

---

<sup>4</sup>Either as a true cancellation of the Zeeman-induced polarization, or due to the intrinsic weakness of the scattering polarization signals used to infer magnetic fields via the Hanle effect.

strengths often coexist within the resolution elements. According to the same observations, kG and sub-kG fields fill only a small fraction of the photospheric volume. In our case the detected magnetic fields occupy only 1% of the total volume (or 4% of the volume if we restrict the estimate to those places with detected signals; see 4.5). In IR observations the fraction increases since the intrinsic field strengths are lower, but still there is enough space for extra weak fields. In particular, those inferred in Hanle effect based determinations of turbulent fields (e.g, Stenflo et al. 1998; Bianda et al. 1998; Bianda et al. 1999).

The scenario described above is very much in favor of a magnetic field with complicated topology, whose properties we are just beginning to glimpse. Two additional results of our study have to be included as part of the complexity. First, we find that a large fraction of the signals correspond to two different polarities in the resolution element (35% of the weakest signals, see Fig. 9). The magnetic field lines of the two magnetic components in the model atmosphere cross the horizontal plane in opposite senses. Second, the bulk magnetic flux of the region is contained in the weakest signals that we detect (see Fig. 8). Moreover, the flux that we find is larger than the fluxes associated to the IN fields in previous works having lower sensitivity (§4.3), indicating that the amount of flux that we detect still is a matter of sensitivity. In other words, a fraction of the existing magnetic structures is missing. They will emerge in future measurements with improved sensitivity and better spatial resolution analyzed through the proper diagnostic technique.

Should the quiet region that we observe be typical of the rest of the Sun, its flux would be comparable to (and even larger than) the flux crossing the solar surface in the form of active regions at any time during the solar cycle maximum (some  $10^{24}$  Mx). Do quiet Sun fields play an active role during the cycle? We simply do not know. However, since the flux (and presumably energy) that they contain is so important, it is difficult to discard any potential influence. Keep in mind that we detect only a fraction of the existing flux.

This work uses a new inversion technique to extend the study by SAL to weaker signals. The conclusions expressed here are very much in the line of those already found by SAL, except that here we rest on a larger statistical basis. In particular, the velocity flows that we find (§4.4) are also of the kind that fits the typical plage and network asymmetries in a MISMA context (Sánchez Almeida 1997). Most of the magnetized mass is at rest but there is also strong co-spatial downflows that produces the observed asymmetric line shapes.

The mechanism that concentrates magnetic fields to form kG fields remains unclear. We do not detect weak field strength precursor regions with enough magnetic flux to produce typical network magnetic concentrations ( $10^{17}$  Mx –  $10^{18}$  Mx). Sánchez Almeida (2001) proposed that the concentration process takes place in patches of much smaller fluxes ( $10^{16}$  Mx), which are then gathered by the super-granular converging flows to create the regular

network structures that we observe. If so, there should be a population of structures of low flux but already concentrated kG fields. We believe that they begin to show up in the upper left corner of Figure 7. The finding of such population demands the existence of concentration mechanisms able to efficiently operate with low flux structures, like the thermal relaxation process described by Sánchez Almeida (2001).

As we pointed out above, the investigation of the quiet Sun fields is still in a developing phase. Each new contribution suggests observations to either confirm previous findings or explore conjectures. In this sense, the above results naturally convey to simultaneous and co-spatial IR and visible observations. They will prove or discard the co-existence of sub-kG and kG field strengths that we support. They also would allow to witness the concentration process of low flux structures. Such observation requires high sensitivity to both kG and sub-kG field strengths, which can be attained by the simultaneous use of IR and visible spectral lines. On the other hand, we conjecture that the quiet Sun fields may participate in the global solar magnetic cycle playing a significant but still unknown role. Monitoring of the quiet Sun magnetism along the cycle using sensitive spectro-polarimeters is eagerly needed<sup>5</sup>.

Much of the efforts to assess the reliability of the results were inspired by discussions with Bruce Lites. He also provided the data employed here. Thanks are due to Arturo López Ariste and Javier Trujillo Bueno for suggestions to improve the manuscript. This work has been partly funded by the Spanish DGES under project 95-0028-C. It has been carried out within the EC-TMR European Solar Magnetometry Network.

---

<sup>5</sup>This may be an ideal task for the vector magnetograph of the synoptic instrument SOLIS; <http://www.nso.noao.edu/solis/>.

## REFERENCES

- Bianda, M., Stenflo, J. O., & Solanki, S. K. 1998, *A&A*, 337, 565
- . 1999, *A&A*, 350, 1060
- Cattaneo, F. 1999, *ApJ*, 515, L39
- Collados, M. 2001, in *ASP Conf. Ser.*, Vol. 236, *Advanced Solar Polarimetry – Theory, Observations, and Instrumentation*, ed. M. Sigwarth (San Francisco: ASP), in press
- Delbouille, L., Roland, G., & Neven, L. 1973, *Photometric Atlas of the Solar Spectrum* (Liège: Institut d’Astrophysique de L’Université de Liège)
- Elmore, D. F., Lites, B. W., Tomczyk, S., Skumanich, A., Dunn, R. B., Schuenke, J. A., Streander, K. V., Leach, T. W., Chambellan, C. W., Hull, H. K., & Lacey, L. B. 1992, *Proc SPIE*, 1746, 22
- Grossmann-Doerth, U., Keller, C. U., & Schüssler, M. 1996, *A&A*, 315, 610
- Harvey, J. & Livingston, W. 1969, *Sol. Phys.*, 10, 283
- Keller, C. U., Deubner, F.-L., Egger, U., Fleck, B., & Povel, H. P. 1994, *A&A*, 286, 626
- Kneer, F. & Trujillo-Bueno, J. 1987, *A&A*, 183, 91
- Lin, H. 1995, *ApJ*, 446, 421
- Lin, H. & Rimmele, T. 1999, *ApJ*, 514, 448
- Lites, B. W., Elmore, D. F., Seagraves, P., & Skumanich, A. 1993, *ApJ*, 418, 928
- Lites, B. W., Leka, K. D., Skumanich, A., Martínez Pillet, V., & Shimizu, T. 1996, *ApJ*, 460, 1019
- Livingston, W. C. & Harvey, J. W. 1971, in *IAU Symp.*, Vol. 43, *Solar Magnetic Fields*, ed. R. Howard (Dordrecht: Reidel), 51
- Livingston, W. C. & Harvey, J. W. 1975, *BAAS*, 7, 346
- López Ariste, A. 2001, in *ASP Conf. Ser.*, Vol. 236, *Advanced Solar Polarimetry – Theory, Observations, and Instrumentation*, ed. M. Sigwarth (San Francisco: ASP), in press
- Rees, D. E., López Ariste, A., Thatcher, J., & Semel, M. 2000, *A&A*, 355, 759

- Sánchez Almeida, J. 1997, *ApJ*, 491, 993
- Sánchez Almeida, J. 1998, in *ASP Conf. Ser.*, Vol. 155, *Three-Dimensional Structure of Solar Active Regions*, ed. C. E. Alissandrakis & B. Schmieder (San Francisco: ASP), 54
- . 2000, *ApJ*, 544, 1135
- . 2001, *ApJ*, 556, in press
- Sánchez Almeida, J., Landi Degl’Innocenti, E., Martínez Pillet, V., & Lites, B. W. 1996, *ApJ*, 466, 537
- Sánchez Almeida, J. & Lites, B. W. 2000, *ApJ*, 532, 1215
- Sánchez Almeida, J. & Trujillo Bueno, J. 1999, *ApJ*, 526, 1013
- Schrijver, C. J. & Harvey, K. L. 1994, *Sol. Phys.*, 150, 1
- Sigwarth, M., Balasubramaniam, K. S., Knölker, M., & Schmidt, W. 1999, *A&A*, 349, 941
- Skumanich, A., Lites, B. W., Martínez Pillet, V., & Seagraves, P. 1997, *ApJS*, 110, 357
- Smithson, R. C. 1975, *BAAS*, 7, 346
- Socas-Navarro, H. 2001, in *ASP Conf. Ser.*, Vol. 236, *Advanced Solar Polarimetry – Theory, Observations, and Instrumentation*, ed. M. Sigwarth (San Francisco: ASP), in press
- Socas-Navarro, H., López Ariste, A., & Lites, B. W. 2001, *ApJ*, 553, 949
- Spiegel, E. A. 1957, *ApJ*, 126, 202
- Stenflo, J. O. 1973, *Sol. Phys.*, 32, 41
- Stenflo, J. O., Keller, C. U., & Gandorfer, A. 1998, *A&A*, 329, 319
- Stenflo, J. O. & Lindegren, L. 1977, *A&A*, 59, 367
- Stix, M. 1991, *The Sun* (Berlin: Springer-Verlag)
- Wang, J., Wang, H., Tang, F., Lee, J. W., & Zirin, H. 1995, *Sol. Phys.*, 160, 277
- Yi, Z., Jensen, E., & Engvold, O. 1993, in *ASP Conf. Ser.*, Vol. 46, *The Magnetic and Velocity Fields of Solar Active Regions*, ed. H. Zirin, G. Ai, & H. Wang, San Francisco, 232
- Zhang, J., Lin, G., Wang, J., Wang, H., & Zirin, H. 1998, *A&A*, 338, 322



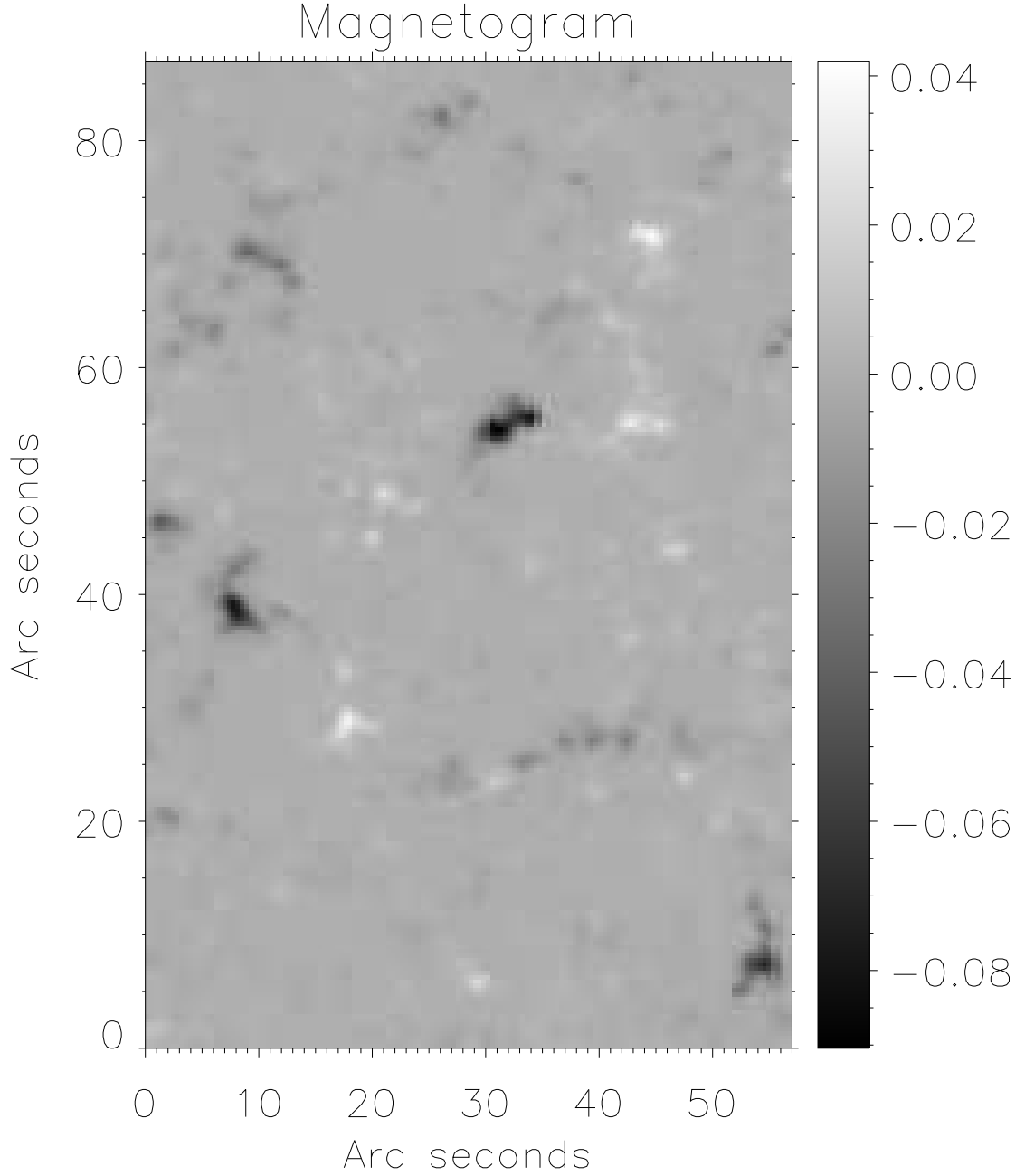


Fig. 1.— Magnetogram of the observed region. The network stands out clearly. We display the degree of circular polarization in the blue wing of the Fe I line at  $6302.5 \text{ \AA}$ . The vertical bar gives the equivalence between grade of grey and polarization. The spatial coordinates of the map are in arc seconds for the lower left corner.

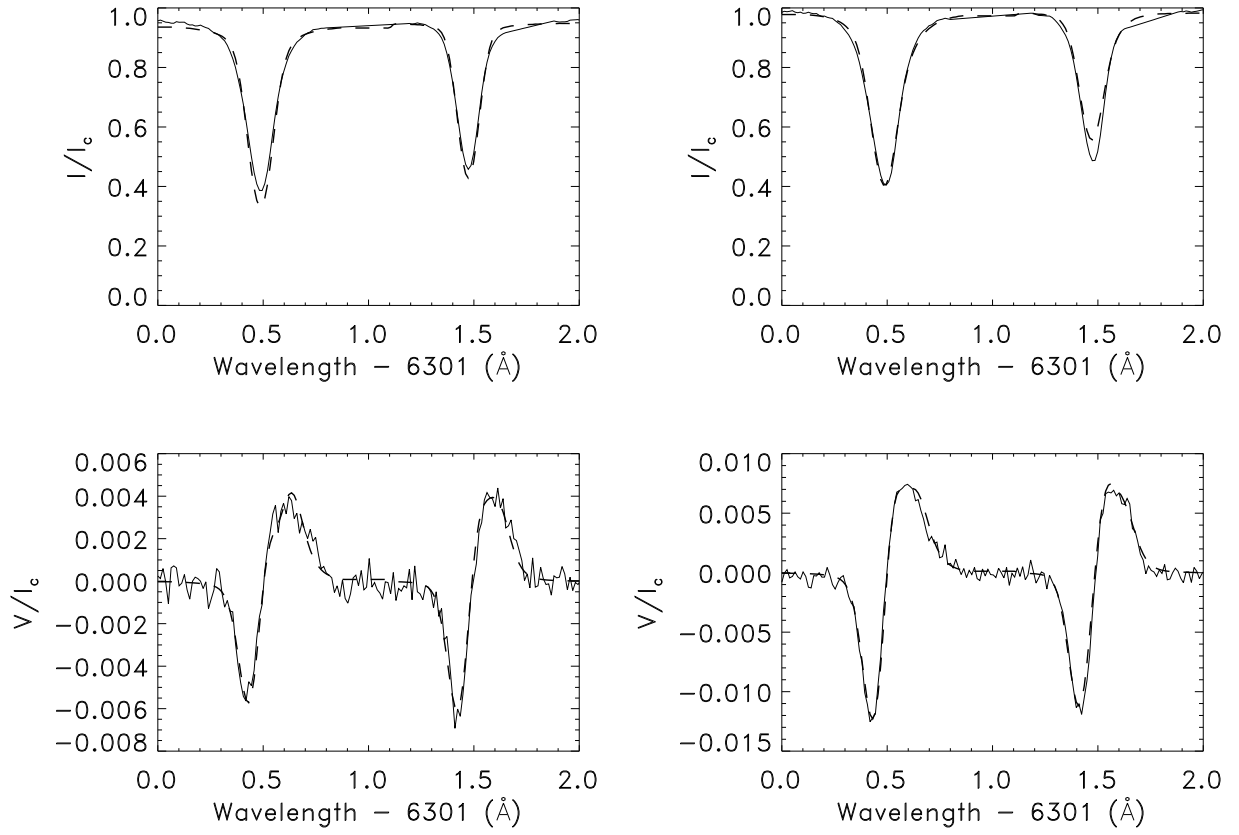


Fig. 2.— Examples of fits to profiles with relatively high signals. Solid lines: observations. Dashed lines: fits. Each column corresponds to a point on the Sun. Stokes  $I$  and  $V$  are normalized to the quiet Sun continuum intensity  $I_c$ . Wavelengths are given in Å from 6301 Å.

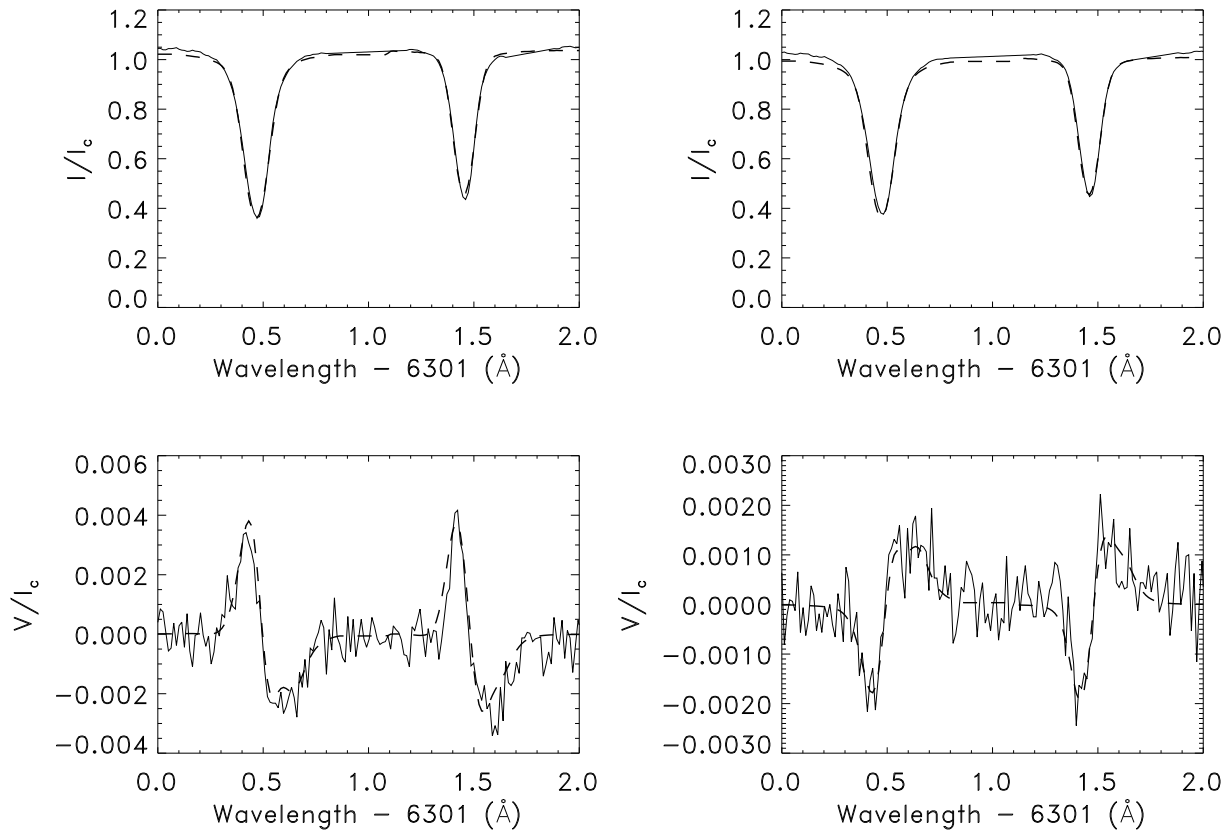


Fig. 3.— Examples of fits to profiles with very low signals. Solid lines: observations. Dashed lines: fits. For the other symbols, see Figure 2.

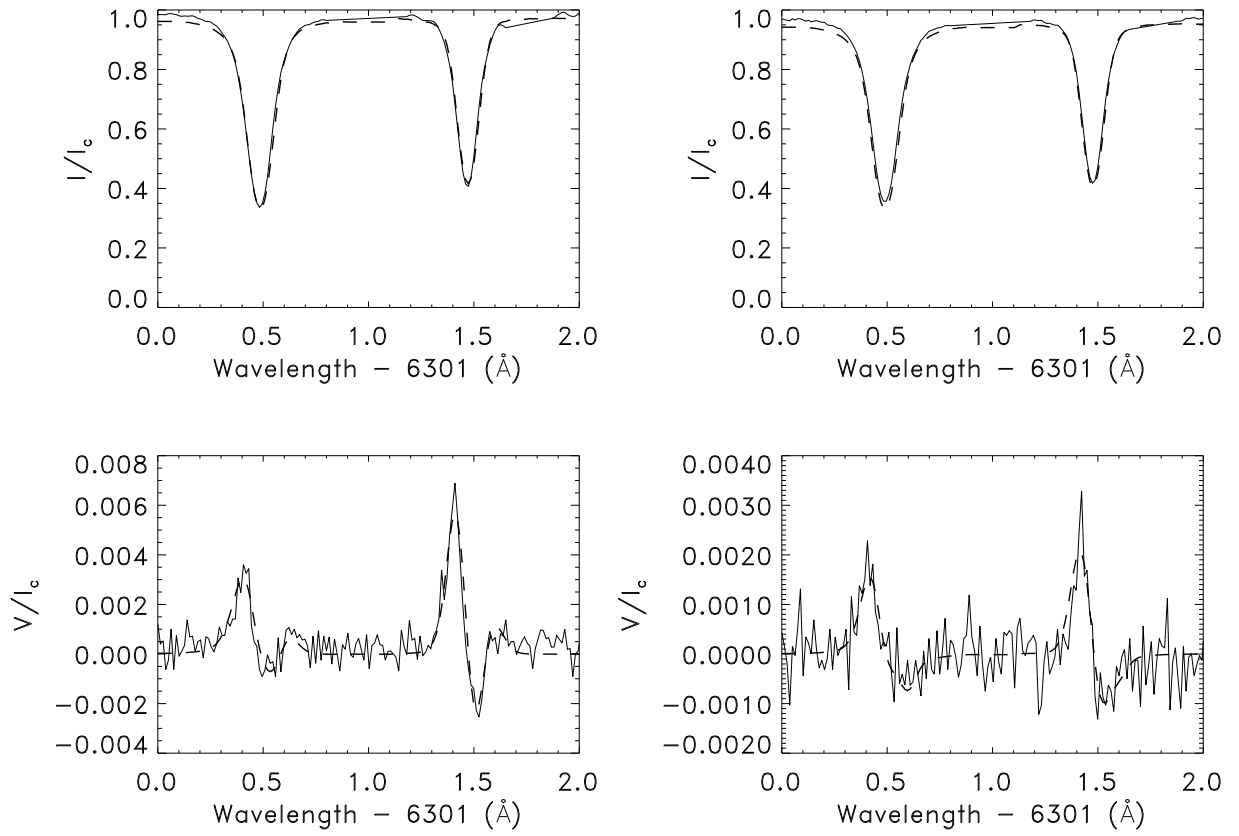


Fig. 4.— Examples of fits to extremely asymmetric profiles. Solid line: observations. Dashed line: fits. For the other symbols, see Figure 2.

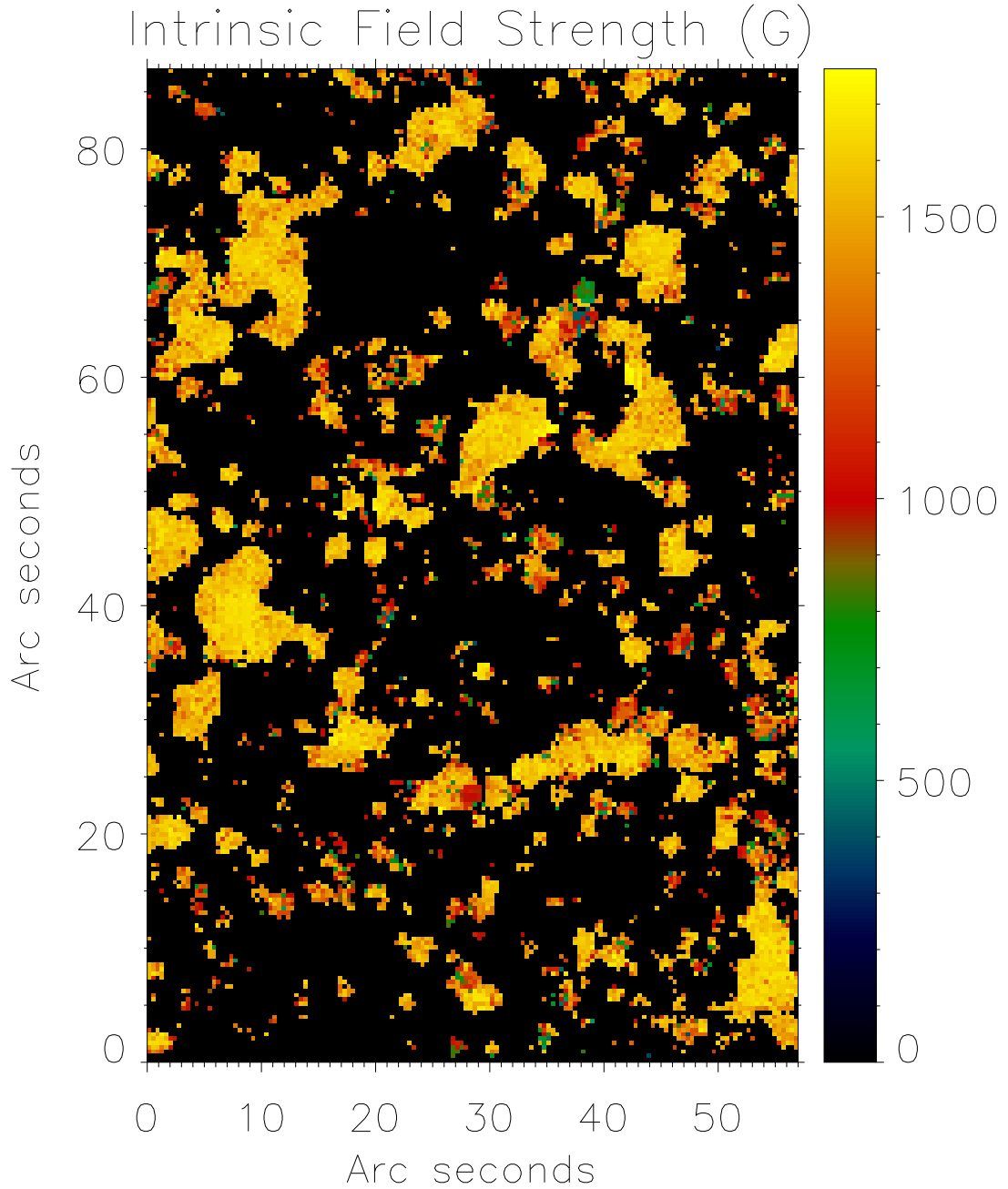


Fig. 5.— Average unsigned magnetic field strength at a height corresponding to the base of the unmagnetized photosphere (i.e., where the total pressure amounts to  $1.3 \times 10^5 \text{ dyn cm}^{-2}$ ). Even inside the network cells, most of the pixels harbor kG field strengths. The vertical bar shows the equivalence between colors and field strengths. Points with polarization below the threshold have been set to zero. The spatial coordinates of the map are in arc seconds.

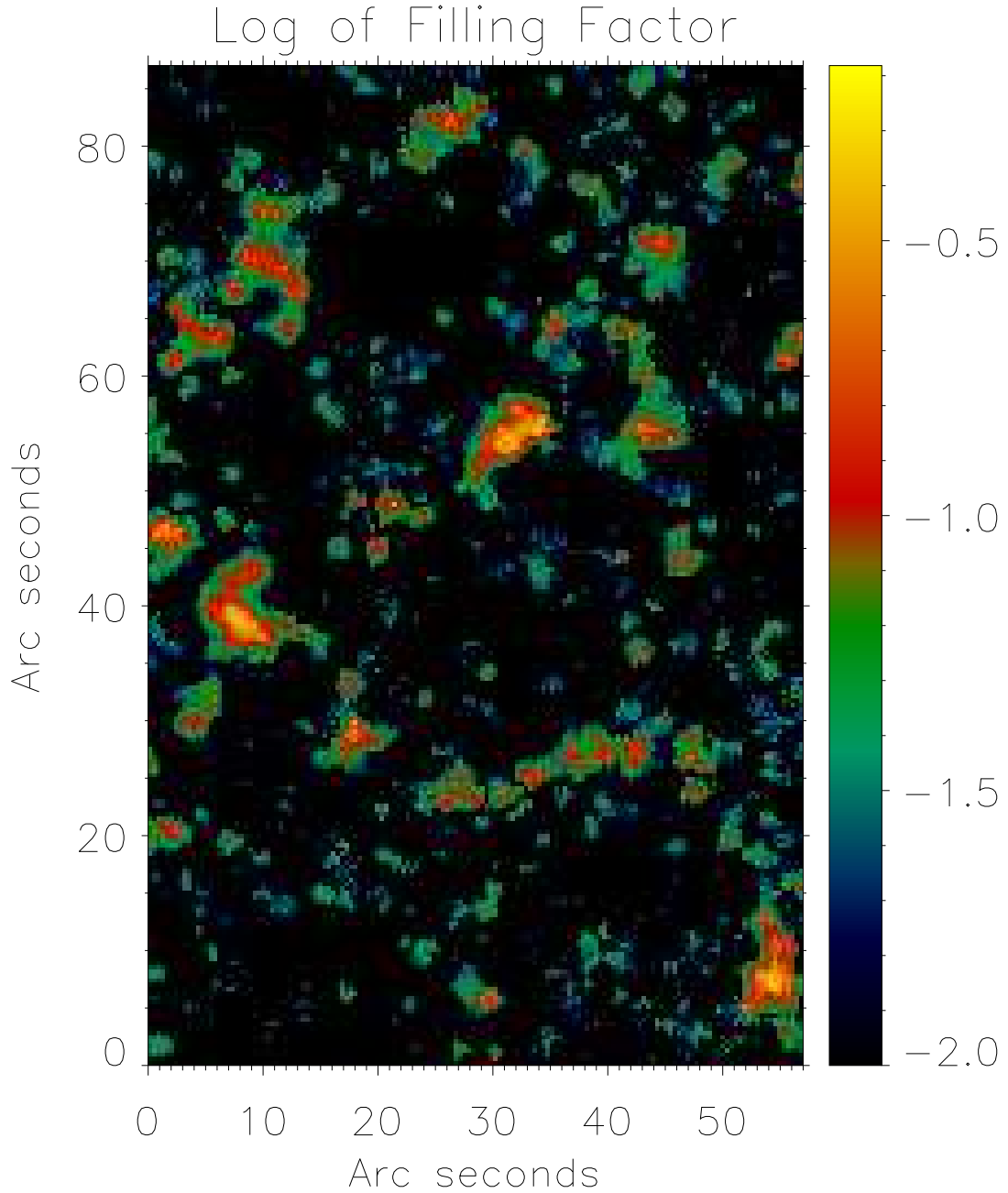


Fig. 6.— Fraction of atmospheric volume occupied by magnetic fields at a height corresponding to the base of the unmagnetized photosphere (i.e., where the total pressure amounts to  $1.3 \times 10^5 \text{ dyn cm}^{-2}$ ). The vertical bar shows the equivalence between colors and occupation fractions, which is given in a logarithmic scale to evidence IN fields. Points with polarization below the threshold have been set to -2. The spatial coordinates of the map are in arc seconds.

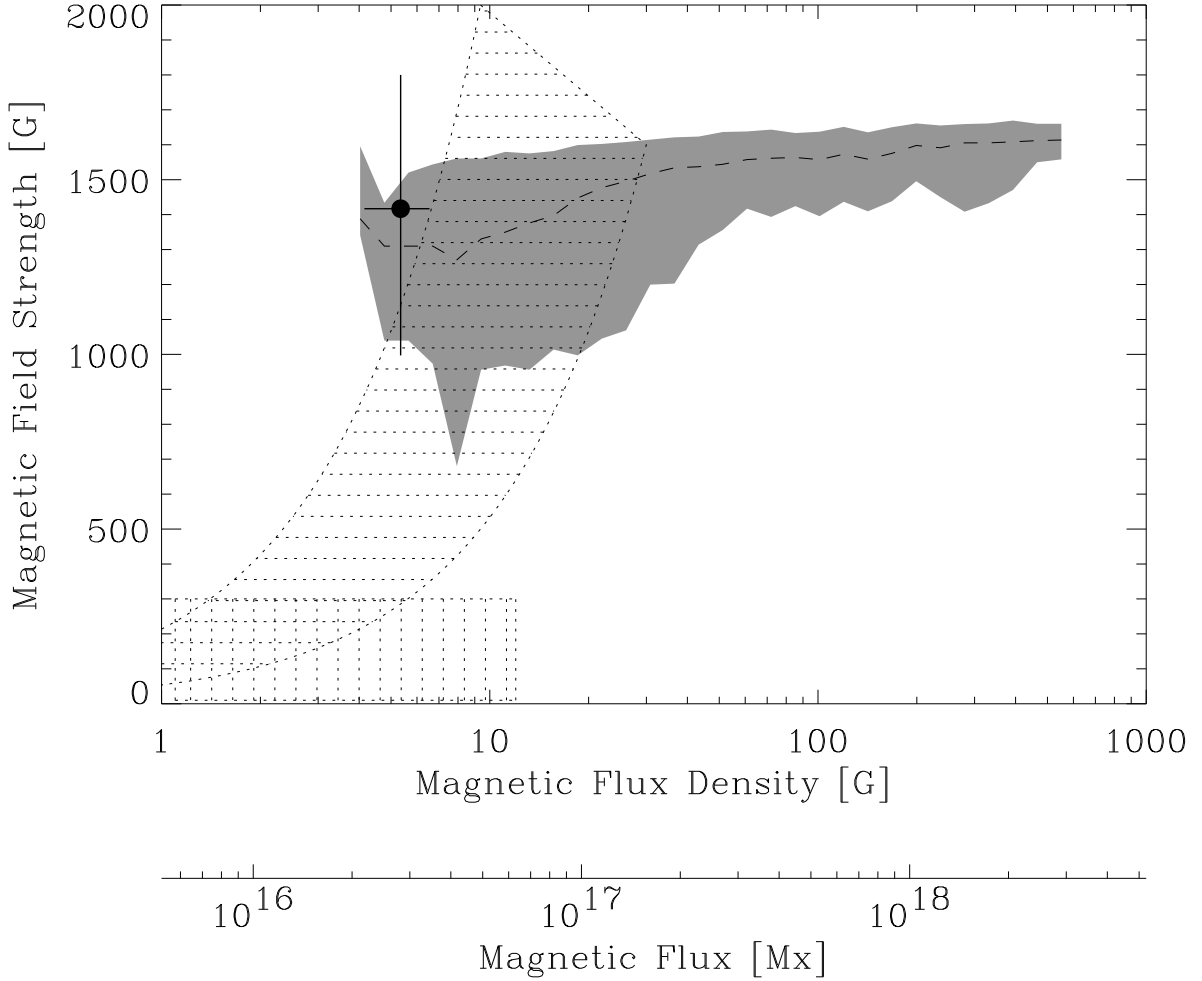


Fig. 7.— Magnetic field strength as a function of the magnetic flux density. The horizontally hashed region corresponds to the limits observed using the Fe I IR line at  $15648 \text{ \AA}$  by Lin (1995) and Lin & Rimmele (1999). The box in the lower left corner marks the results independently obtained by Collados (2001) using the same line (the region in the plot includes 80 % of the observed signals). The analysis of this work leads to the shaded region, which represents the mean (dashed line) as well as the standard deviation above and below the mean (shaded area). The point with error bars was derived by Sánchez Almeida (2001), using part of the dataset analyzed here. The scale of magnetic flux has been computed assuming an angular resolution of  $1''$ .

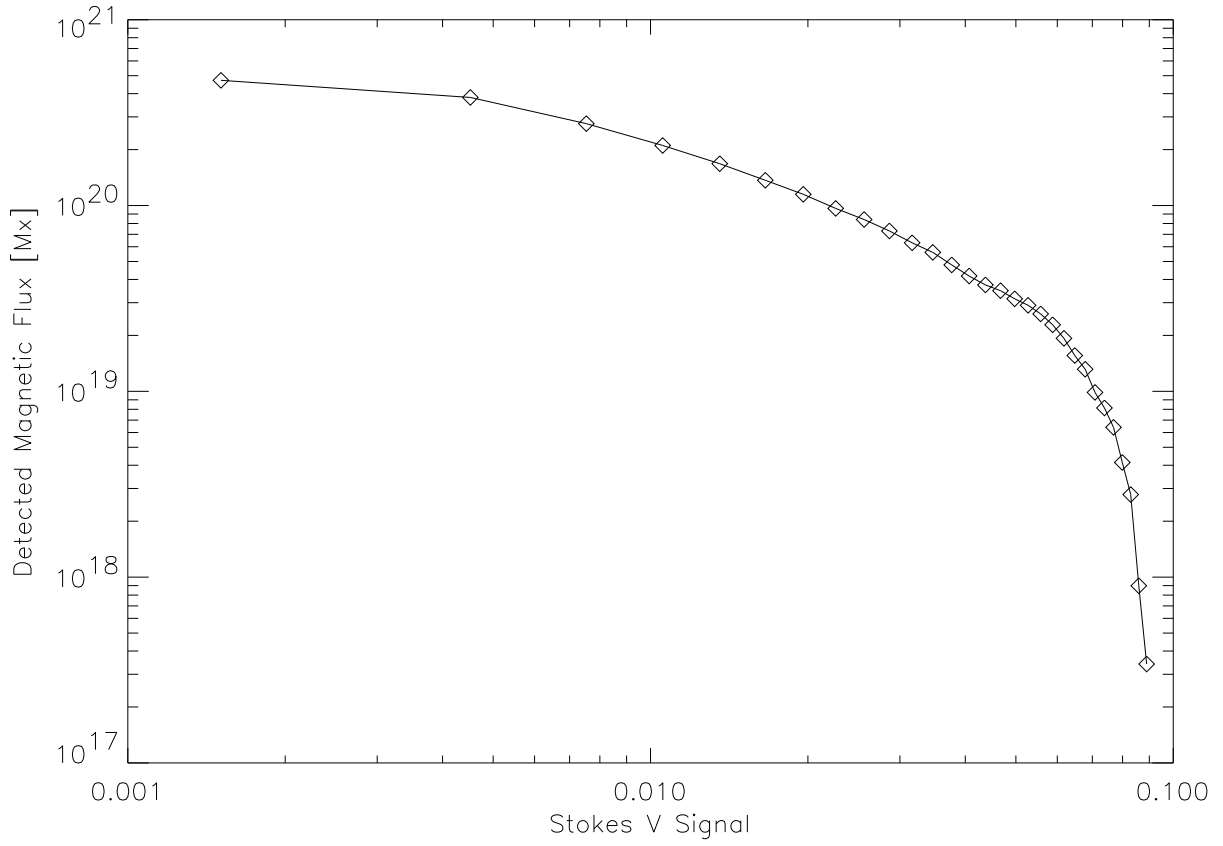


Fig. 8.— Magnetic flux in the region considering all the pixels with signals stronger than the abscissa. The total unsigned flux steadily increases as one considers weaker signals, with no clear signs of saturation for the weakest ones analyzed here. The Stokes  $V$  signals are measured in the same units as the magnetogram in Figure 1.



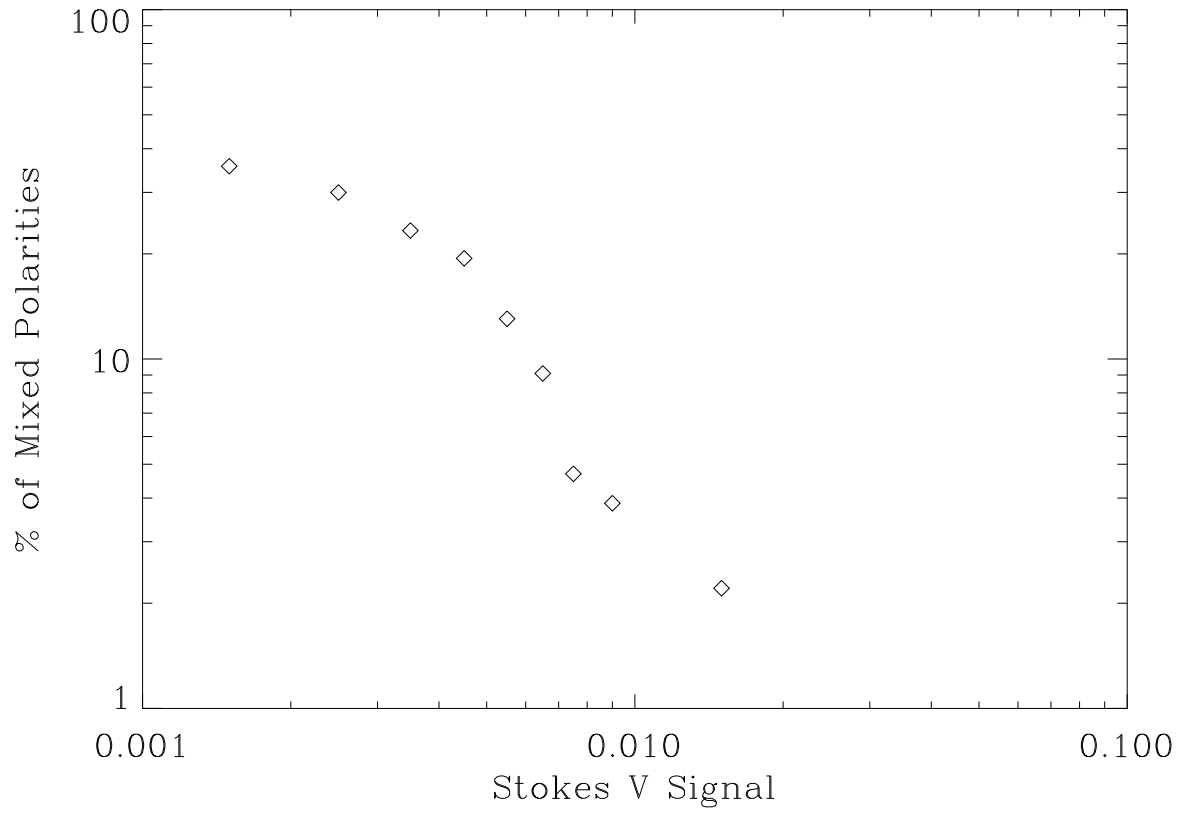


Fig. 9.— Percentage of pixels having two different polarities in the resolution element as a function of the Stokes  $V$  signal. The percentage reaches some 35% for the weakest polarization signals analyzed here.

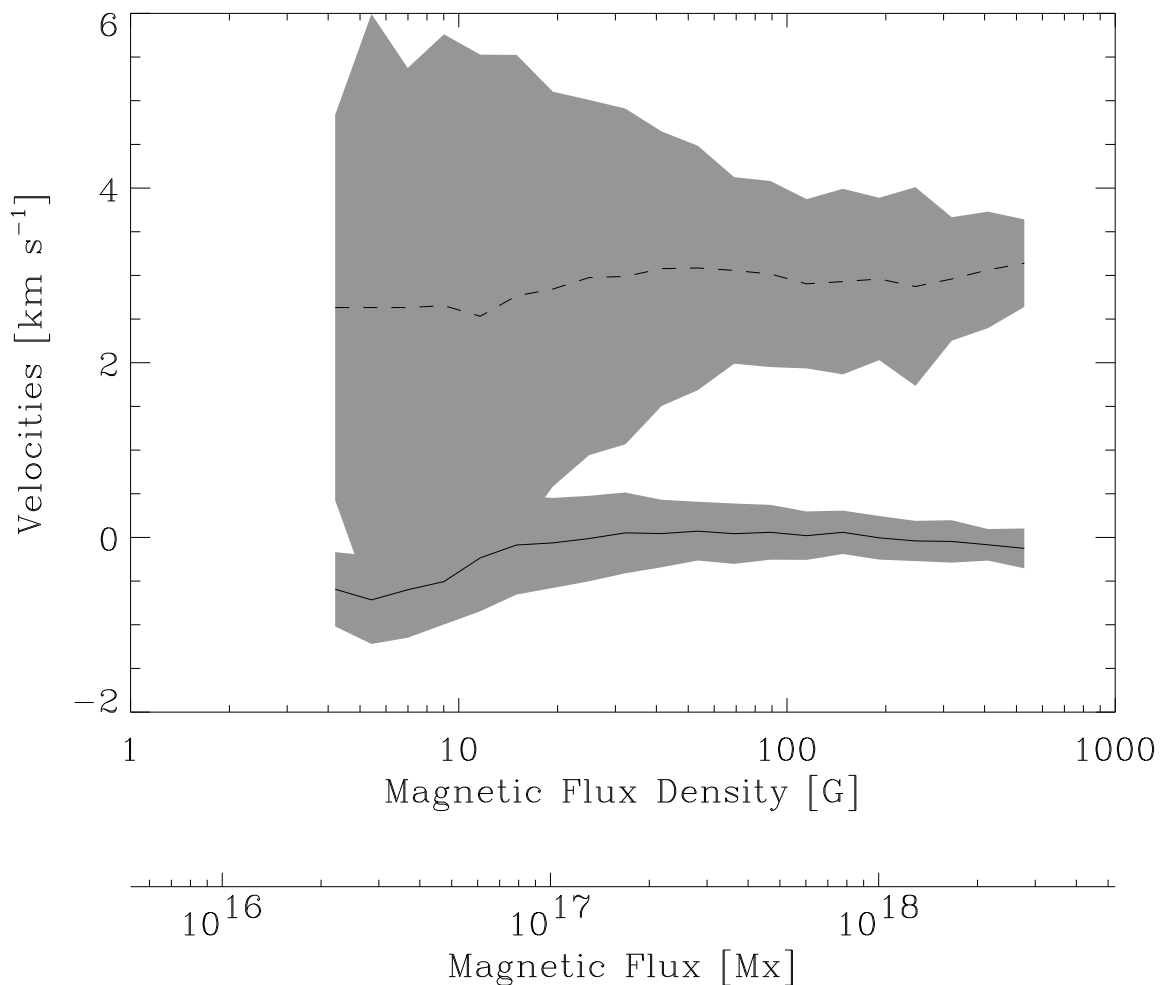


Fig. 10.— The solid (dashed) line represents the mean of the velocities in the first (second) magnetic component at a height corresponding to the base of the quiet photosphere. It is represented versus the unsigned magnetic flux density in the resolution element. The shaded areas correspond to the mean plus-minus the standard deviation of the distribution. Positive velocities are red shifts or downflows. The magnetic flux axis has been computed as for Figure 7

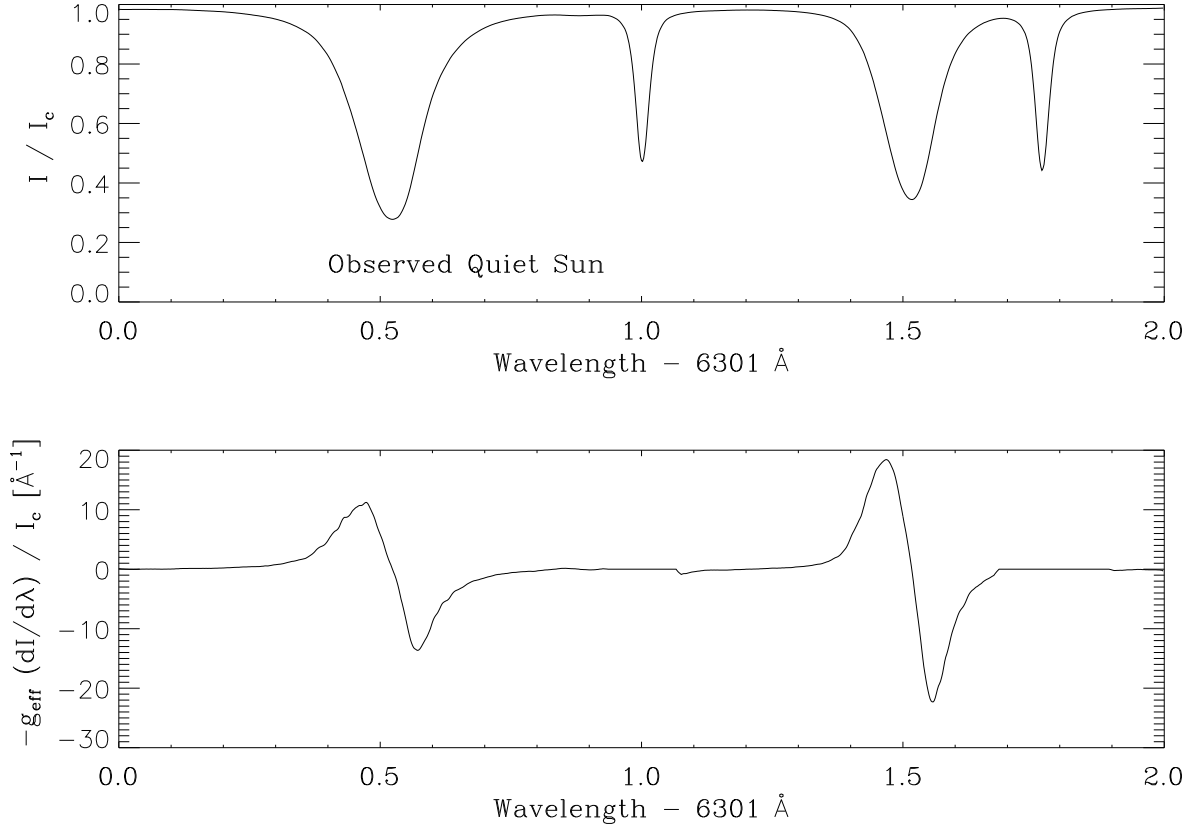


Fig. 11.— Top: Stokes  $I$  profiles of Fe I 6302.5 Å and Fe I 6301.5 Å observed in the quiet Sun at the solar disk center (Delbouille et al. 1973). If the spectral lines are formed under weak magnetic field conditions, the relative amplitude of the Stokes  $V$  signals should be given by the weak field approximation, i.e., the derivative of the Stokes  $I$  profiles times the effective Lande factor of the line (bottom). The signal to be expected in Fe I 6302.5 Å is some 60% larger than that produced by Fe I 6301.5 Å. Wavelengths are given in Å from 6301 Å.

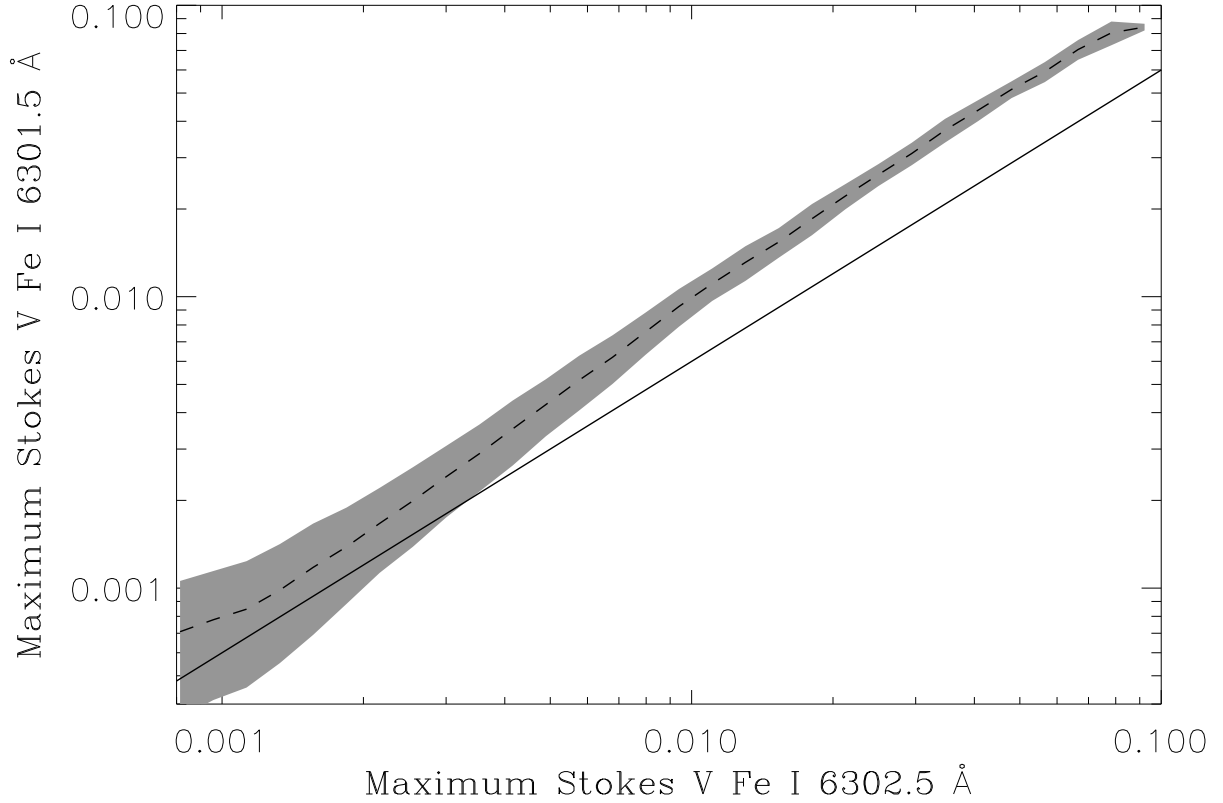


Fig. 12.— Scatter plot of the maximum Stokes  $V$  signals observed in the two Fe I lines subject to analysis. The shaded region corresponds to the mean plus and minus the standard deviation among the Fe I 6301.5 Å signals with a given Fe I 6302.5 Å signal. The mean of this distribution is represented by the dashed line. The solid line shows the relationship to be expected if the magnetic field were intrinsically weak (see Fig. 11). Most of the observed ratios correspond to strong fields, i.e., to points above this ratio.